Advances in Industrial and Manufacturing Engineering 5 (2022) 100105

Contents lists available at ScienceDirect

Advances in Industrial and Manufacturing Engineering

journal homepage: www.sciencedirect.com/journal/advances-in-industrial-and-manufacturing-engineering

Influence of WAAM-CMT deposition parameters on wall geometry

A.L.B. Novelino, G.C. Carvalho, M. Ziberov *

University of Brasília, Faculty of Technology, Department of Mechanical Engineering, 70910-900, Brasília, DF, Brazil

ARTICLE INFO

Keywords:
Additive manufacturing
WAAM
CMT
Parameters selection
Geometry analysis

ABSTRACT

The Wire and Arc Additive Manufacturing has called attention due to its potential in allowing the buildup of high integrity metallic parts using the commonly available welding robots in the industry. However, such a technology still presents some challenges, mainly related to obtaining optimal deposition parameters, which result in consistent layer geometry which leads to the robot and the welding power source programming. In this sense, the objective of this work is to analyze the influence of the parameters in bead and multi-layer wall geometries fabricated by the Cold Metal Transfer process to select the configurations that result in the best deposition control. The study was carried out in four steps: (i) deposition of single beads on plate, varying wire feed speed and travel speed that would result in stable and sound beads; (ii) deposition of five layer walls, considering both unidirectional and bidirectional path strategies, with and without stops between layers; (iii) deposition of ten and twenty layer walls, refining deposition parameters; and (iv) deposition of a one hundred layer wall, with the best parameter configuration among the previously tested, with bidirectional continuous strategy. The results showed that the geometry produced with a mean current of 62 A and torch travel speed of 8 mm/s along each layer and 24 mm/s on the transition between layers generated the best results, considering the natural cooling conditions. Also, the bidirectional path deposition presented the most regular geometries, when compared to the unidirectional strategy.

1. Introduction

Additive Manufacturing (AM) has become a high-demand process over the years since its evolution expanded the application to different materials and complex geometries. The 4.0 Industry also introduced new technologies that helped the process automation in production lines to reduce fabrication time and production costs (Wu et al., 2018). Automotive, aerospace, medical, and civil construction segments are applying AM technologies to reduce material waste and generate optimized and customized products. (Ngo et al., 2018). Also the benefits of merging additive and subtractive manufacturing compared to pure subtractive manufacturing is highlighted by Campatelli et al. (2020), which compared the methods for steel blade manufacturing and achieved a material economy of almost 2 kg for a 0.847 kg component. The energy efficiency for the additive-subtractive method was higher, with up to 50 MJ energy save.

One of the AM technologies designed for metal fabrication is the Wire and Arc Additive Manufacturing (WAAM), that consists of a Metal Additive Manufacturing process which uses metallic wire as additive material and an electric arc as the source of energy for melting and depositing the metal along the pre-programed path resulted from slicing of the three-dimensional (3D) virtual model of the part. This concept can be adapted from different welding methods, such as conventional Gas Metal Arc Welding (GMAW) and its variant Cold Metal Transfer (CMT), Gas Tungsten Arc Welding (GTAW), and Plasma Arc Welding (PAW). WAAM can also be used with different types of metals, such as ER70S-6 mild steel wire, used by Nagasai et al. (2022) for fabrication of cylindrical geometries using GMAW and CMT power supplies. Also, the titanium alloy Ti–6Al–4V was employed by Artaza et al. (2020) using the PAW method. Furthermore, nickel-based superalloys such as Inconel 625, Inconel 718, and some Ni–Ti alloys were used with the GMAW and the PAW processes (Dhinakaran et al., 2020).

However, deposition physics and parameters set up for the WAAM process still need to be better comprehended and optimized along the deposition period. Also, it is necessary to control the heat balance on the part under construction throughout the deposition process, so that it is possible to obtain some control on the microstructural and macrostructural results. Other problems that need attention are the presence of contaminants and poor atmosphere control in the deposition region, that can result in high porosity and other defects (Wu et al., 2018). As listed

* Corresponding author.
E-mail address: mziberov@unb.br (M. Ziberov).

https://doi.org/10.1016/j.aime.2022.100105
Received 30 May 2022; Received in revised form 2 November 2022; Accepted 17 November 2022
Available online 19 November 2022
2666-9129/© 2022 The Authors. Published by Elsevier B.V. This is an open access article under the CC BY-NC-ND license (http://creativecommons.org/licenses/by-nc-nd/4.0/).

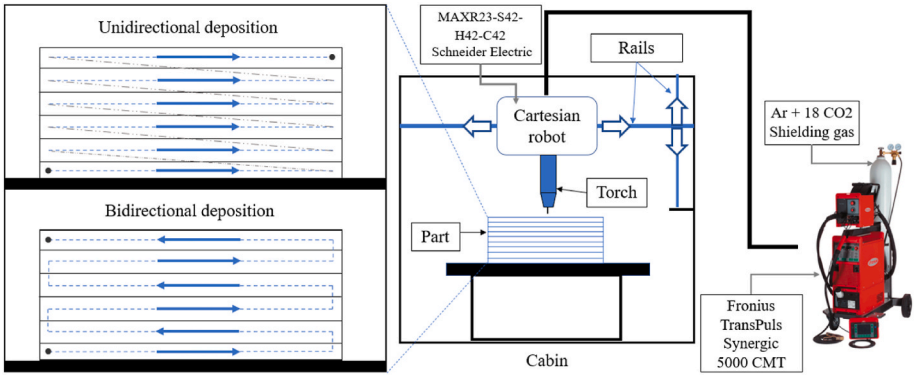

Fig. 1. Setup used for wall deposition and path strategies applied for the deposition.

by Jafari et al. (2021), some WAAM common issues are residual stress and distortions, caused by thermal-induced strains, further to gas pores that weaken mechanical strength, and contribute to cracks appearance/growth that harm fatigue resistance. Also, out-of-control material flow, which are resulted from inadequate deposition parameters, and allied to poor heat balance can lead to defects such as humping, which affects the layer profile and, thus, results in a deposited geometry that does not match the 3D virtual geometry programed.

The geometry accuracy for WAAM fabricated parts was approached by Laghi et al. (2019), focusing on stainless steel planar plates and tubular structures fabricated with continuous deposition for a product development by MX3D company. The authors emphasized the importance of controlling material deposition, reducing surface roughness and lack of straightness of the fabricated elements, comparing the digital model of with the real elements. The surfaces defects and irregularities were characterized and measured, reaching in a 13% larger thickness than the nominal value. For cross sectional area measurements, the authors obtained a 5% smaller cross-sectional area from the nominal reference from the digital model. The authors concluded reaffirming that geometric characterization is necessary to assess the most suitable printing parameters and minimize discrepancies.

To explore the effect of deposition strategy in WAAM, Aldalur et al. (2020) used the GMAW method to compare different deposition strategies for high deposition rates using ER70S-6 wire with a 1.2 mm diameter. The authors applied overlapping and oscillating torch paths to manufacture wall samples and compared macrostructure, microstructure, and hardness. The overlapped wall presented higher hardness values along all its length and height, with center wall hardness of 146 HV for the overlapped wall and 136 HV for the oscillated wall. The overlapped wall also achieved greater Ultimate Tensile Strength (UTS) and Yield Strength (YS) compared with the oscillated sample, with horizontal UTS and YS for the overlapped sample with 498 $\pm$ 8 MPa and 368 $\pm$ 12 MPa, and oscillated sample with 478 $\pm$ 6 MPa and 354 $\pm$ 13 MPa, respectively. The authors explains that the higher mechanical properties from the overlapping strategy samples occurs because of the smaller grain size obtained in the resulting microstructure (Aldalur et al., 2020).

Liberini et al. (2017) focused their study on the selection of process parameters for the GMAW deposition method using ER70S-6, with bidirectional deposition and cooling time of 60 s between each layer. The authors manufactured fifteen layers walls with six parameters configurations, using fixed current value of 60 A and merging torch travel speed from 300 mm/min, 375 mm/min, and 450 mm/min, and voltage with 11.7 V and 13.1 V. The comparative analysis showed a higher height for the sample with 11.7 V and 300 mm/min speed rate compared to the others, with the heat input of 11,707 J/m. The authors identified, based on microhardness analysis, 3 different zones, represented as: (a) a lower zone characterized by a roughly equiaxed grains, resulting in a microhardness of 225 HV; (b) a middle zone, with 150 HV and (c) an upper zone, with 275 HV. The middle and the upper zones were characterized by a lamellar microstructure. According to the authors, the discrepancy of the hardness values in middle and upper zones is related to the predominant bainite structure presented in upper zone, whereas the middle zone presented bainite/ferritic mixed structure (Liberini et al., 2017).

Nagasai et al. (2022) also used ER70S-6 wire to fabricate cylindrical components using the GMAW and CMT processes. The objective of the study was to evaluate and compare both processes based on metallurgical and mechanical analyses. The study reached optimal parameters for both processes, with the CMT reaching a higher feed speed of 7 m/min compared to GMAW (6.7 m/min). The authors compared both processes based on the deposition of single beads using different WFS configurations: 6 m/min, 7 m/min and 7.5 m/min. On higher wire feed speed values, it was outstanding the higher material deposition control that results from the CMT process, with lower heat affected zone and thinner bead. Comparing the cylindrical geometries manufactured, using a current configuration of 229 A for GMAW, and 200 A for CMT, both samples presented a similar average thickness, with 7.8 $\pm$ 2 mm for the GMAW and 7.3 $\pm$ 2 mm for the CMT. To analyze the mechanical properties, Nagasai et al. (2022) manufactured 6 specimens (3 samples for the bottom region and 3 for the top region). For the CMT, the tensile properties, impact toughness, and hardness were higher compared to the GMAW. The authors explained that the higher properties of the CMT process are mainly due to the fast cooling of the process, which applied for the ER70S-6, formed microstructure with bainite and acicular ferrite in the top region and perlite immersed in ferrite grains in the bottom region (Nagasai et al., 2022).

Considering the problems reported in the literature, especially the one highlighted by Laghi et al. (2019) about the importance of geometric characterization for industry application, and focusing the promising applicability by CMT process and the difficulty in defining the appropriate deposition parameters for the desired geometry, the present study evaluates the influence of WAAM process parameters on the ER70S-6 material deposition by means of the CMT process and compare the geometry obtained along all length. A simple planar vertical wall, formed by overlapping single bead horizontal layers was chosen as the geometry to be deposited, comparing different deposition strategies. The main objective was to obtain parameters and a deposition strategy configuration that generates a well-structured AM part, based on geometry analyses of deposited walls, contributing to the understanding of its correlation, and favoring future application of the method.

2. Material and methods

The WAAM system used for deposition the samples were presented in Fig. 1. It consisted of a *Fronius TransPuls Synergic* 5000 CMT power source and a 3-axes cartesian robot (*Schneider Electric MAXR23-S42-H42-C42*) with a working volume of 740 $\times$ 570 $\times$ 500 mm and 0.1 mm

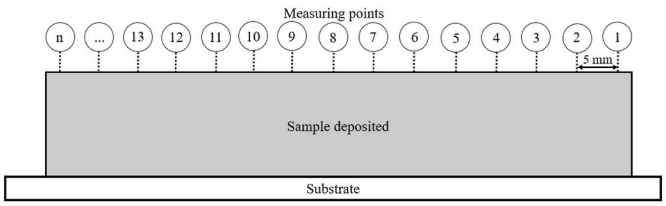

Fig. 2. Measure procedure for samples geometric analyses.

resolution. As additive material, a mild steel ER70S-6 wire with 1.2 mm diameter was used, deposited over AISI 1020 steel plates, using Ar+18% CO_2 as shielding gas at a 15 l/min flow rate. The initial contact tip-to-work distance (CTWD) determined for all samples was 12 mm.

Three deposition strategies were used for sample analyses: the unidirectional deposition with interlayer temperature control (ITC), the bidirectional deposition with ITC and the continuous bidirectional deposition (without ITC). The three strategies compared allows a better understanding of the material flow and it reflects on the final geometry for the fabricated parts. Also, the interlayer temperature control used was 30 °C to avoid overheating effect during layers overlapping for multilayer samples.

For the measurement procedure, as showed in Fig. 2, all samples were separated into measuring points, distanced by 5 mm along the sample length. The samples with 70 mm length were divided into fourteen measuring points, and the 160 mm length samples were separated into thirty-one measuring points. The weld gauge USHS-4 (0.1 mm resolution and 12 mm for nominal scale) and vernier caliper Mitutoyo (0.05 mm resolution and 150 mm for nominal scale) were used for measuring the samples. All samples' widths and heights were acquired at the defined measuring points, with average and standard deviation (99.73% probability) values obtained with five measurements. For interlayer temperature control, the temperature was approximated after each layer deposition by means of a digital laser thermometer KLX (0.10 °C resolution and −50 °C–380 °C range).

3. Results and discussion

The samples were organized in groups, according to the number of beads/layers deposited: (a) single beads, (b) 5 layers, (c) 10 layers, (d) 20 layers and (e) a final sample with 100 layers. The samples were evaluated according to surface quality (presence of superficial defects and weld spatter), the geometry (height and width), and the heat input, calculated from process power input (average current times average voltage), torch travel speed, and path strategy. The qualitative results in those three categories were rated from 1 (lower quality) to 5 (higher quality).

3.1. Single bead samples

The 70 mm length single beads were deposited using different current configurations. The power source synergic curve used had an arc correction factor of 5% to guarantee arc stability during deposition. The parameters selected were the current and the Wire Feed Speed (WFS). For this group, eight samples were produced, with the nominal parameters introduced to power source and robot Torch Travel Speed (TTS) parameters shown in Table 1. The current configuration presented were also applied for other groups, in order to analyze it for different deposition scenarios.

Based on group analysis, the samples with 65 A, 112 A, and 131 A and TTS of 6 mm/s presented better geometry aspects based on qualitative analysis and measurements, according to the results registered in Fig. 3a. The highlighted samples are shown in Fig. 3b, outlining their difference in width. All measuring points from those samples are represented in Table 2, with the average values for each point and the mean height and width for three samples.

Using the comparative analysis of the samples indicated in Fig. 3a and the geometric analysis, it was concluded that the bead submitted to 170 A or higher resulted in low reinforcement height and high substrate penetration, indicating that the heat input obtained for the TTS of 6 mm/s exceeds the ideal parameters, by increasing melt penetration and harming bead morphology. Once the other groups tends demand better

Table 1
Nominal deposition parameters configurations introduced to power source.

Deposition parameters										
Current config. (A)	65	112	131	170	189	229	266	277	131	131
Voltage (V)	19.1	21.0	20.5	23.2	24.6	25.5	28.5	29.1	20.5	20.5
WFS (m/min)	2.0	3.7	5.2	6.6	7.6	8.7	10.9	10.9	5.2	5.2
TTS (mm/s)	6								12	18
Heat input (J/mm)	206.9	392.0	447.6	657.3	774.9	973.2	1263.5	1343.5	223.8	149.2

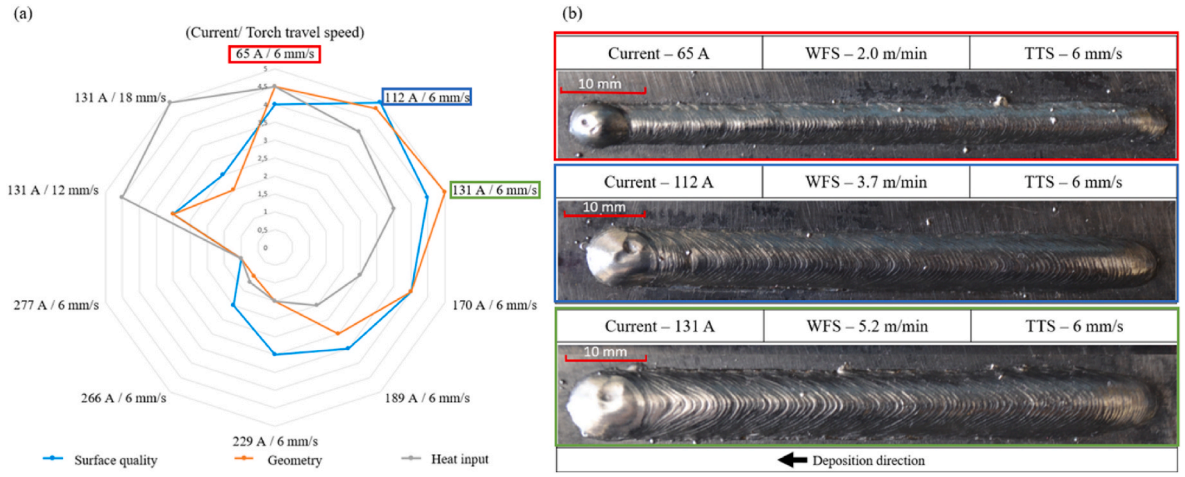

Fig. 3. (a) Qualitative and comparative analysis of simple bead samples. (b) Samples deposited with TTS of 6 mm/s and current of 65 A, 112 A, and 131 A.

Table 2
Measurements for single bead samples with 65 A, 112 A and 131 A.

Single bead – 65 A/6 mm/s															
Height (mm)															
MP	**1**	**2**	**3**	**4**	**5**	**6**	**7**	**8**	**9**	**10**	**11**	**12**	**13**	**14**	**AV**
$\overline{X}$	1.60	1.96	1.84	1.76	1.78	1.74	1.68	1.66	1.76	1.76	1.92	1.86	1.88	1.98	**1.80**
SD	0.47	0.17	0.17	0.17	0.39	0.17	0.14	0.27	0.40	0.17	014	0.17	0.25	0.54	**0.11**
Width (mm)															
$\overline{X}$	4.46	4.44	5.26	4.82	5.22	5.02	5.16	5.00	5.06	5.28	4.86	5.18	4.88	5.10	**4.98**
SD	0.17	0.55	0.27	0.25	0.14	0.39	0.40	0.21	0.17	0.14	0.40	0.14	0.14	0.21	**0.27**
Single bead – 112 A/6 mm/s															
Height (mm)															
MP	**1**	**2**	**3**	**4**	**5**	**6**	**7**	**8**	**9**	**10**	**11**	**12**	**13**	**14**	**AV**
$\overline{X}$	1.62	2.58	2.70	2.30	2.12	2.20	2.28	2.06	2.10	2.14	2.12	2.14	2.22	2.20	**2.20**
SD	0.39	0.39	0.21	0.21	0.14	0.30	0.33	0.27	0.21	0.17	0.14	0.34	0.25	0.21	**0.25**
Width (mm)															
$\overline{X}$	5.42	7.16	7.74	7.48	7.66	7.40	7.54	7.46	7.36	7.18	7.36	7.56	7.40	7.70	**7.32**
SD	0.39	0.17	0.17	0.68	0.46	0.21	0.17	0.17	0.55	0.39	0.50	0.17	0.21	0.21	**0.57**
Single bead – 131 A/6 mm/s															
Height (mm)															
MP	**1**	**2**	**3**	**4**	**5**	**6**	**7**	**8**	**9**	**10**	**11**	**12**	**13**	**14**	**AV**
$\overline{X}$	2.82	3.00	2.80	2.80	2.80	2.72	2.38	2.46	2.32	2.26	2.24	2.06	1.90	1.88	**2.46**
SD	0.14	0.21	0.21	0.30	0.21	0.25	0.33	0.46	0.33	0.17	0.17	0.16	0.30	0.25	**0.37**
Width (mm)															
$\overline{X}$	6.02	8.26	8.70	8.70	8.45	8.62	8.62	8.62	8.74	8.70	8.70	8.72	8.78	8.96	**8.47**
SD	0.39	0.59	0.47	0.37	0.62	0.39	0.44	0.25	0.46	0.42	0.47	0.25	0.25	0.46	**0.72**

MP – Measuring points along the sample.
$\overline{X}$ – Mean value at MP after 5 measurements.
SD – Standard deviation (99.73%).
AV – Average of all MPs.

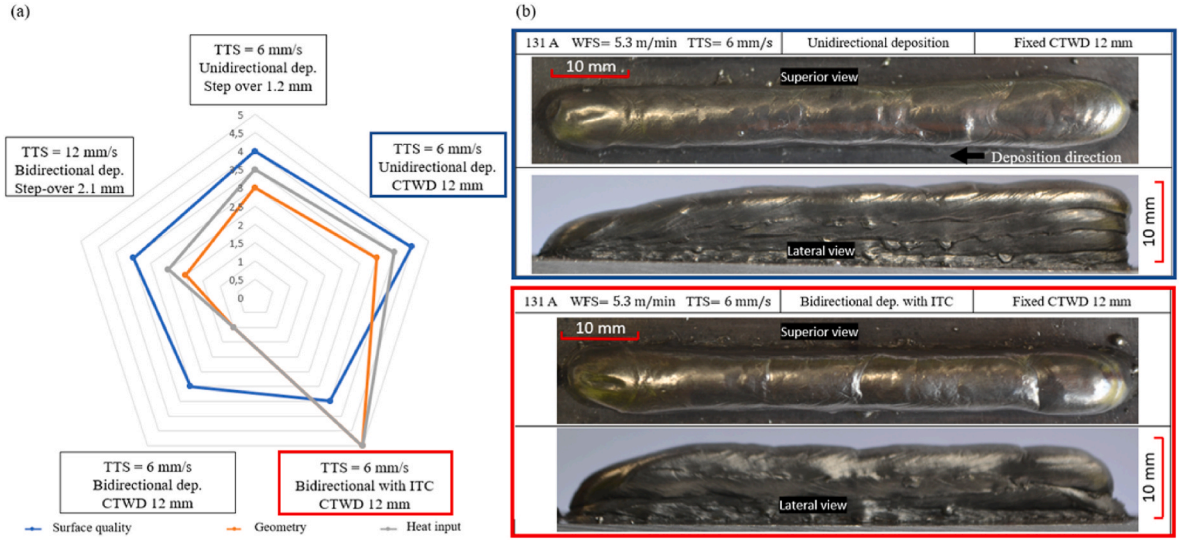

Fig. 4. (a) Qualitative and comparative analysis of five-layer walls. (b) Samples deposited with TTS of 6 mm/s and unidirectional and bidirectional deposition with Interlayer temperature control.

material controlling, all the configurations of 170 A or above were ignored for the further analysis.

The sample which used TTS of 18 mm/s presented width and length oscillations, which denotes the "pre-humping" effect. According to DebRoy et al. (2018), the humping effect happens when the liquid metal at the top of the molten pool is lower than shielding gas velocity, leading to a hydrodynamic instability called Kelvin Helmholtz (KH) instability. In terms of process parameters, the effect indicates that TTS is too high, and it causes arc instability and oscillation in the melting pool (Yamba et al., 2019). Based on the results, the current level of 170 A or higher and TTS above 18 mm/s were not used. The bead geometries showed a thinner and stable width compared to the single bead deposited by Nagasai et al. (2022), which deposited the same wire for GMAW and CMT processes, although the larger WFS used by the authors resulted in a higher bead compared to the highlighted ones from Fig. 3b.

3.2. *Five-layers walls*

After selecting the parameters from the previous single bead depositions, attempts of building walls by overlapping sequential beads were started. Primarily, it was studied the buildup of 70 mm length walls structured with 5 layers, aimed at listing the initial effects presented for

Table 3
Measurements for the five-layers walls with unidirectional and bidirectional with ITC deposition.

Five-layer wall – 131 A/6 mm/s (Unidirectional deposition)									
Height (mm)									
MP	**1**	**3**	**5**	**7**	**9**	**11**	**13**	**14**	**AV**
$\overline{X}$	10.68	11.02	10.46	10.08	9.28	9.02	5.96	4.92	**9.31**
SD	0.25	0.44	0.34	0.14	0.39	0.25	0.46	0.39	**1.84**
Width (mm)									
$\overline{X}$	7.58	9.06	8.62	8.18	7.54	7.88	8.16	8.62	**8.32**
SD	0.39	0.17	0.14	0.39	0.17	0.25	0.17	0.14	**0.56**
Five-layer wall – 131 A/6 mm/s (Bidirectional deposition with ITC)									
Height (mm)									
MP	**1**	**3**	**5**	**7**	**9**	**11**	**13**	**14**	**AV**
$\overline{X}$	8.20	9.98	10.10	10.06	10.08	10.16	9.80	8.12	**6.68**
SD	0.21	0.25	0.30	0.27	0.25	0.17	0.56	0.72	**0.25**
Width (mm)									
$\overline{X}$	6.72	8.56	8.04	8.24	7.90	8.06	9.12	9.08	**7.14**
SD	0.58	0.17	0.27	0.17	0.21	0.27	0.33	0.14	**0.27**

MP – Measuring points along the sample.
$\overline{X}$ – Mean value at MP after 5 measurements.
SD – Standard deviation (99.73%).
AV – Average of all MPs.

this type of manufacturing that would lower geometry quality. Also, it was considered the maintenance of CTWD, to keep arc stability and stable melt pool behavior during the deposition of higher layers. Interlayer temperature control was also analyzed as it reflects on the cooling process and heat input cycles.

For the group of five-layer walls, the current configuration of 131 A presented in Table 1 was used. Two configurations of TTS were tested: 6 mm/s and 12 mm/s. Three deposition strategies were carried out: Continuous bidirectional, bidirectional with ITC, and unidirectional with ITC. The comparison is presented in Fig. 4a, with the parameters used for each deposition strategy. The interlayer control temperature resulted in more stable height along the length, obtaining a higher grade, besides of the control of heat input. Fig. 4b shows the difference in the results of the deposition strategies, with the samples using the same TTS (6 mm/s) and initial CTWD (12 mm). It is possible to observer that both samples presented a tail end of left side due to the same start deposition point and temperature increase during deposition process, which expand molten pool, lowering effective height of the layer at the point. The unidirectional sample presented a standard deviation from the average height of 1.84 mm among all specimens taken along the wall height, compared to 0.25 mm for the bidirectional sample, as shown in Table 3. However, the bidirectional one presented a region with contraction cavity, due to material shrinkage, which lowered surface quality. Despite of it, the configuration with bidirectional and ITC deposition presented regular values for height and width.

During the deposition process for the five-layers wall group, the drop in productivity was noticeable when using manual adjustment of the torch Z-coordinate (vertical movement) to maintain the CTWD fixed, which proved to be not efficient for real applications. As mentioned by Laghi et al. (2019), for engineering applications, such larger structural elements, it is important that WAAM process is able to have high deposition velocity, and also keep an acceptable accuracy for geometry of printed parts, in order to maintain fabrication viability. Thus, the next samples deposited used a step-over distance (vertical up movement at the end of each deposited layer) without manual correction to find a configuration that prioritizes productivity.

Some researchers already studied these aspects, intending to minimize torch distance error by implementing an automatic correction. Xiong and Zhang (2014) proposed the implementation of laser vision sensors to monitor layer height during deposition and automatically

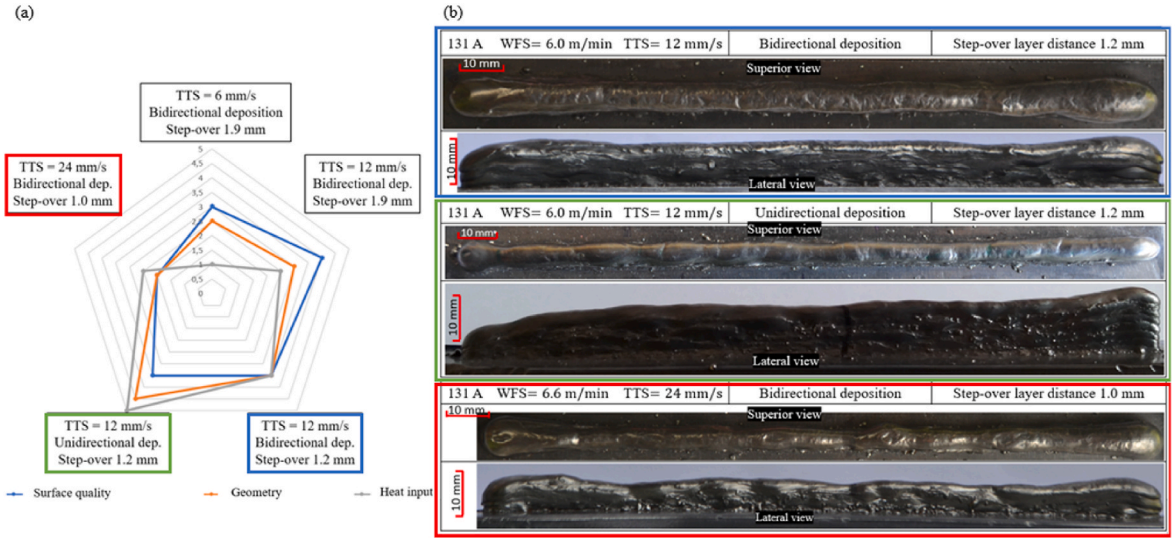

Fig. 5. (a) Qualitative and comparative analysis of ten-layer walls. (b) Samples with TTS of 6, 12, and 24 mm/s and unidirectional and bidirectional deposition.

Table 4
Measurements for the ten-layers walls with unidirectional and bidirectional deposition with step over distance of 1.0 mm and 1.2 mm.

Ten-layer wall - 131 A/12 mm/s (Bidirectional deposition and step over distance 1.2 mm)												
Height (mm)												
MP	**1**	**4**	**7**	**10**	**13**	**16**	**19**	**22**	**25**	**28**	**31**	**AV**
$\overline{X}$	9.12	11.12	10.14	9.92	10.06	10.66	10.58	10.66	9.94	10.54	11.96	**10.46**
SD	0.49	0.58	0.34	0.14	0.27	0.17	0.25	0.55	0.27	0.27	0.17	**1.82**
Width (mm)												
$\overline{X}$	9.60	9.18	8.60	7.56	7.36	7.38	7.70	7.50	8.24	7.76	10.88	**8.30**
SD	0.30	0.14	0.21	0.17	0.17	0.14	0.21	0.21	0.17	0.17	0.14	**3.42**
Ten-layer wall - 131 A/12 mm/s (Unidirectional deposition and step over distance 1.2 mm)												
Height (mm)												
MP	**1**	**4**	**7**	**10**	**13**	**16**	**19**	**22**	**25**	**28**	**31**	**AV**
$\overline{X}$	15.66	15.58	14.1	13.52	13.58	13.42	12.00	12.36	12.70	12.50	10.86	**12.94**
SD	0.40	0.39	0.21	0.14	0.54	0.49	0.42	0.34	0.30	0.37	0.78	**5.55**
Width (mm)												
$\overline{X}$	5.90	6.80	5.88	5.44	5.56	5.38	6.28	6.16	6.50	6.74	6.34	**6.20**
SD	0.30	0.21	0.25	0.34	0.27	0.25	0.62	0.46	0.37	0.34	0.27	**1.70**
Ten-layer wall - 131 A/24 mm/s (Bidirectional deposition and step over distance 1.0 mm)												
Height (mm)												
MP	**1**	**4**	**7**	**10**	**13**	**16**	**19**	**22**	**25**	**28**	**31**	**AV**
$\overline{X}$	7.00	7.98	5.84	6.92	7.12	6.40	6.96	6.66	6.84	7.42	7.44	**7.00**
SD	0.21	0.14	0.17	0.44	0.33	0.47	0.62	0.27	0.34	0.54	0.92	**2.10**
Width (mm)												
$\overline{X}$	9.20	7.02	5.84	5.70	5.38	5.04	6.30	5.34	6.04	6.64	8.18	**6.31**
SD	0.30	0.14	0.17	0.21	0.25	0.27	0.21	0.17	0.34	0.17	0.39	**3.39**

MP – Measuring points along the sample.
$\overline{X}$ – Mean value at MP after 5 measurements.
SD – Standard deviation (99.73%).
AV – Average of all MPs.

adjust the torch-workpiece distance. Another study from Wang et al. (2021) proposed the implementation of a 3D scanning system alongside thermal sensors for height monitoring. Although reported by the authors as feasible, it is not considered the best approach, when it comes to programming a robot, since the preprogrammed path must be defined based on the expected layer height to be attained during the deposition process. Therefore, the knowledge of the layer height and width that result from a set of deposition parameters is of utmost importance for the deposition planning. Further, some degree of adaptivity can also be included for the robotic deposition system to control the layer height during the process, which would demand the development of strategies for measuring the deposited layer height and to control it by means of varying some of the deposition parameters. However, such control capability still needs more studies to become feasible.

3.3. Ten-layers walls

The third group analysis consisted of ten-layers walls, which were deposited based on the best performed strategies used by previous groups. In this group, the current configuration used was 131 A, varying TTS between 6 mm/s, used in previous group, 12 mm/s and 24 mm/s. The ten-layer walls were deposited using the two strategies with higher quality from five-layers group: the continuous bidirectional and the unidirectional with ITC. Also, as observed in five-layers walls, the samples length showed to be small, resulting in poor cooling of the sample during deposition. Therefore, the layer length was extended to 160 mm with the objective to increase interlayer time and improve cooling efficiency.

All configurations and qualitative analyses for the group are presented in Fig. 5a, with the unidirectional sample presenting a higher geometry quality and the sample with TTS of 24 mm/s with the worst geometry. Among the 5 configurations applied, 3 configurations highlighted are introduced and compared in Fig. 5b. The sample with unidirectional deposition presented a stable width along all length, with a mean width of 6.20 ± 1.70 mm. However, the deposition strategy was influenced by a higher height standard deviation, with a value of 12.94 ± 5.55 mm, as shown in Table 4 alongside some measuring points along the length. The effect was also reported by Rodrigues et al. (2019) for the deposition of 1 mm diameter ER110S-G wire with GMAW process, where the authors comment about the importance of deposition strategy to control molten pool and compensates height difference between the start and the end of the layer due to different temperatures during deposition. The authors also mention the issue of height difference accumulation, resulting in different CTWD along the sample and lead to defects related to material deposition.

The bidirectional sample, otherwise, with the same TTS and current, presented a higher average width of 8.30 ± 3.42 mm, and a lower but stable height, with average of 10.46 ± 1.82 mm. The sample deposited with TTS of 24 mm/s is also presented in Fig. 5b and indicates that the configuration generates irregular material flow, causing the humping effect mentioned in the first group. Another effect highlighted by Deb-Roy et al. (2018) that can be clearly seen for the sample is the “balling effect”, caused by Plateau Raleigh capillary instability, which represents the molten pool elongation and the effect of separation caused due to high TTS speed. Due to the results, the TTS parameter was targeted at values up to 12 mm/s for the next group to avoid irregular geometry.

The ten-layers wall analysis showed that geometry quality of the samples increases due to the 160 mm length, leading to better cooling efficiency during the overlapping period that reduces the heat concentration occurred in the 70 mm length samples. About path strategy, as mention by Jafari et al. (2021), the selected strategy has strong influence on bead geometry and height maintenance for model generation, which can be determined by samples comparison between unidirectional and bidirectional. The bidirectional samples achieved better height consistency, also stablished for five layers samples and, despite for Martina et al. (2012) based on titanium alloy Ti–6Al–4V analysis using plasma process, the authors related the same behavior for the unidirectional deposition samples for the analysis of layer height.

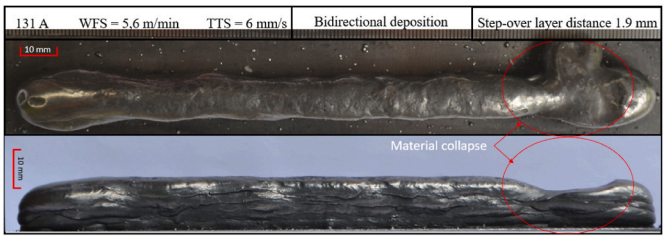

Fig. 6. Material collapse presented for the sample with 131 A and TTS of 6 mm/s.

The sample presented in Fig. 6 was deposited using 131 A and TTS of 6 mm/s as deposition parameters, which resulted in collapse of molten pool due to high heat input and poor interlayer cooling, proving that current configurations above 131 A that used 6 mm/s for torch speed are susceptible to lack of material deposition control. Rodrigues et al. (2019) emphasize that heat concentration leads to a higher material runoff from the molten pool. Based on author's analysis for ER110S-G material, the worst geometry was obtained from the TTS of 3.9 mm/s compared to the sample with 9 mm/s for the current configuration of 95 A. Based on authors analysis with the group deposited, and poor quality obtained from the TTS of 6 mm/s for the current configuration of 131 A or higher using natural cooling, once the layer collapse indicated that the heat input exceeds the limit for decent formability.

Also comparing with Rodrigues et al. (2019), the authors verified that a higher speed configuration of 12 mm/s resulted in better geometry, as can be compared between the sample in Fig. 5b and the collapsed one in Fig. 6. To avoid material collapse, it was decided that for the group of twenty-layers walls, the TTS of 6 mm/s was restricted only for the current configuration of 65 A presented in Table 1 due to the lower heat input.

3.4. Twenty-layers walls

Based on the results from previous groups, two current configurations were used (65 A and 110 A), reducing heat input to obtain a higher control of the molten pool to obtain thinner layer width. All samples of the group were fabricated using bidirectional deposition, once the strategy achieved more stable height for previous groups, and fixed step-over distance to increase productivity. The parameters used are presented in Fig. 7a, with 3 samples deposited, with the objective to analyze the correction of CTWD during the deposition for different TTS values. The first sample applied the current configuration of 65 A and TTS of 6 mm/s with a step-over distance of 1.0 mm. The second sample used the same configuration with TTS of 8 mm/s and a step over of 1.2 mm and the third sample applied a current configuration of 110 A and TTS of 12 mm/s with a step over distance of 1.0 mm. All three geometries are shown in Fig. 7b, with superior and lateral views.

All three samples presented regular height, with standard deviation of all the measuring points below 1.5 mm, as shown in Table 5. Considering the width, the sample deposited with 110 A presented the higher standard deviation in the group, with 1.24 mm, compared with 0.67 mm and 0.61 mm for the samples with TTS of 6 mm/s and 8 mm/s respectively, indicating that the optimal configuration is near the 65 A current samples.

From the samples analyses, all deposited walls from the group presented regular geometry, which is related to the current configuration and bidirectional deposition strategy reached by the previous groups. The sample with 62 A and 8 mm/s achieved the thinner width among all three samples, due to the lower heat input, estimated as 155.2 J/mm for the configuration used. The effect also indicates better control of material flow were achieved, which benefits the reduction of crack-like defects, according to Seow et al. (2020), who studied wire arc additive manufacturing of In 718, with different deposition parameters with the objective to characterize the defects. The authors emphasize that the incidence of cracks is mainly related to heat input and path deposition strategy, which generates areas with high heat stress and lead to low geometry quality and high residual stress (Seow et al., 2020).

From the analysis, it is also noticeable that the TTS of 12 mm/s is better for the current configuration of 110 A compared to the configuration with 6 mm/s used for ten-layers walls. The twenty-layer sample deposited with 110 A presented regular height along all length. However, the 65 A configuration still performed better, with higher and thinner walls with slightly lower deviation. The higher height occurs even with the configuration us using lower WFS, as 2.2 m/min compared with 4.2 m/min used for the 110 A sample.

Comparing the 20-layer walls deposited in the present work with the ones obtained by Anand et al. (2022), who applied similar mild steel wire deposited into a twenty-layer wall using GMAW process with current of 110 A, TTS of 5 mm/s, and WFS set as 8 m/min, all geometries were more stable than the GMAW sample, presenting superior surface quality as well, which confirms the higher material control capability

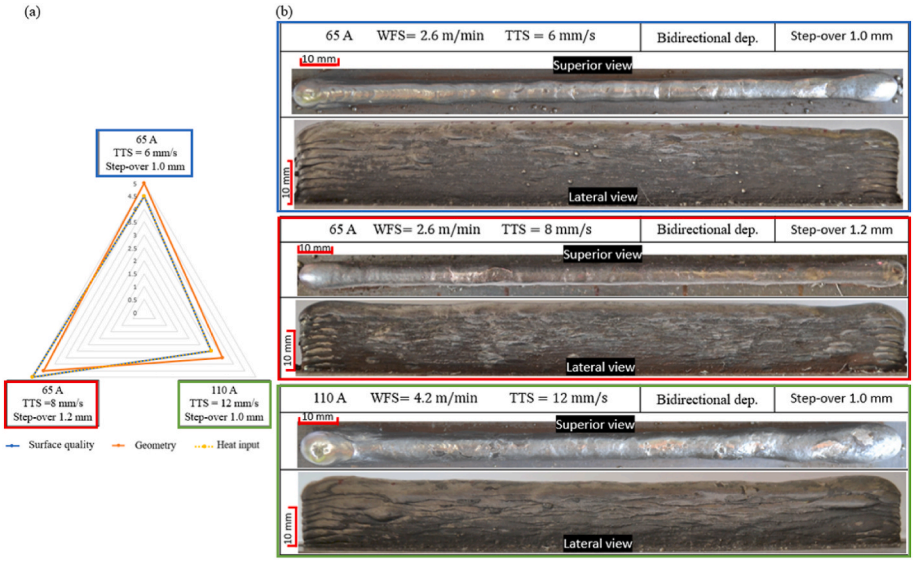

Fig. 7. (a) Qualitive and comparative analysis of twenty-layer walls. (b) Samples with deposition configuration of 65A/TTS 6 mm/s; 65 A/TTS 8 mm/s and 110 A/TTS 12 mm/s.

Table 5
Measurements for the twenty-layers walls with 62 A and 110 A, bidirectional deposition and step over distance of 1.0 mm and 1.2 mm.

Twenty-layer wall - 65 A/6 mm/s (Bidirectional deposition and step over distance 1.0 mm)												
Height (mm)												
MP	**1**	**4**	**7**	**10**	**13**	**16**	**19**	**22**	**25**	**28**	**31**	**AV**
$\overline{X}$	20.22	20.48	20.76	21.20	21.46	21.40	21.28	21.58	20.70	20.78	20.76	**21.01**
SD	0.62	0.25	0.40	0.30	0.40	0.47	0.25	0.25	0.37	0.65	0.34	**1.36**
Width (mm)												
$\overline{X}$	8.74	6.48	6.36	6.40	6.38	6.30	6.14	6.04	6.10	6.62	8.46	**6.56**
SD	0.34	0.39	0.16	0.21	0.13	0.42	0.16	0.16	0.37	0.25	0.16	**0.67**
Twenty-layer wall - 65 A/8 mm/s (Bidirectional deposition and step over distance 1.2 mm)												
Height (mm)												
MP	**1**	**4**	**7**	**10**	**13**	**16**	**19**	**22**	**25**	**28**	**31**	**AV**
$\overline{X}$	18.20	17.98	18.70	18.88	19.02	18.94	18.68	18.98	18.20	17.78	18.80	**18.61**
SD	0.47	0.39	0.37	0.25	0.13	0.16	0.54	0.68	0.47	0.33	0.56	**1.16**
Width (mm)												
$\overline{X}$	7.46	5.68	5.70	5.44	5.80	5.60	5.60	5.88	5.78	6.14	7.44	**5.93**
SD	0.16	0.13	0.00	0.27	0.21	0.30	0.00	0.13	0.25	0.16	0.16	**0.61**
Twenty-layer wall - 110 A/12 mm/s (Bidirectional deposition and step over distance 1.0 mm)												
Height (mm)												
MP	**1**	**4**	**7**	**10**	**13**	**16**	**19**	**22**	**25**	**28**	**31**	**AV**
$\overline{X}$	18.18	18.68	17.60	17.92	17.66	17.82	17.66	17.74	18.28	17.86	18.88	**18.02**
SD	0.33	0.39	0.47	0.33	0.34	0.33	0.62	0.46	0.25	0.62	0.78	**1.35**
Width (mm)												
$\overline{X}$	10.50	10.26	8.94	8.46	7.68	7.38	8.02	7.88	7.92	8.56	10.80	**8.69**
SD	0.70	0.46	0.16	0.16	0.13	0.13	0.25	0.39	0.25	0.50	0.21	**1.24**

MP – Measuring points along the sample.
$\overline{X}$ – Mean value at MP after 5 measurements.
SD – Standard deviation (99.73%).
AV – Average of all MPs.

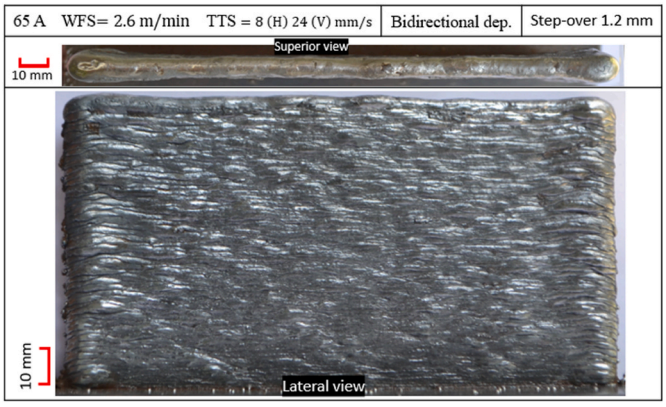

Fig. 8. One-hundred-layers wall deposited with the best parameters determined from all groups' analyses.

from CMT process.

3.5. Final sample – One-hundred-layers wall

Once the previous analyses reached good results with samples submitted to lower heat input, the next step was to produce a one-hundred-layer wall and verify geometric aspects generated by the parameters for larger parts and how deposition would perform for a longer period without temperature control interruption. Even if temperature control benefits geometry quality, normalizing heat input over all sample, the interruption for natural cooling is not productive in terms of manufacturing time and thus it was decided it would not be applied in order to maximize manufacturing productivity.

Based on the twenty-layer wall analysis, the chosen configuration was the current of 65 A and TTS of 8 mm/s, which achieved better geometry with lower heat input. However, the longer deposition process could cause heat stress at extreme points of the wall where the torch changes direction so, as an alternative to minimize the effect, the TTS

Table 6
Measurements for the one-hundred-layer wall with 65 A, 8 mm/s horizontal and 24 mm/s vertical torch travel speeds, bidirectional deposition and step over distance of 1.0 mm.

Hundred-layers wall - 65 A/TTS Horizontal 8 mm/s; Vertical 24 mm/s (step over 1.2 mm)												
Height (mm)												
MP	**1**	**4**	**7**	**10**	**13**	**16**	**19**	**22**	**25**	**28**	**31**	**AV**
$\overline{X}$	84.28	85.08	84.58	85.44	86.08	85.86	86.32	85.22	85.38	85.10	86.20	**85.46**
SD	0.49	0.25	0.13	0.27	0.13	0.16	0.39	0.25	0.25	0.21	0.30	**1.56**
Width (mm)												
$\overline{X}$	9.28	7.44	6.72	6.86	6.50	6.48	7.02	6.76	6.82	7.00	10.10	**7.26**
SD	0.58	0.16	0.13	0.27	0.21	0.13	0.58	0.16	0.58	0.21	0.30	**0.94**

$\overline{X}$ – Mean value at measure point (MP) after 5 measurements.
SD – Standard deviation (99.73%).
AV – Average of all MPs.

was set different for movement directions: the horizontal movement was carried out at 8 mm/s, and the vertical step movement, at 24 mm/s.

The sample obtained from the above configuration is shown in Fig. 8, with an average height and width of 85.46 ± 1.56 mm and 7.26 ± 0.94 mm respectively. Table 6 shows the measurements along the length, demonstrating the regularity of the wall dimensions. No humping or balling effects were detected along the geometry, which indicates that there was not considerable instability for molten pool. However, during wall fabrication, once the deposition process was uninterrupted, it was detected that natural cooling was deficient, once the layers deposited were overheating, mainly after the fiftieth layer. Consequently, the molten pool increased by this point, reducing effective height of the deposited layers and increasing the width by this point. This might have occurred due to the temperature increase within the robot cabin, which might have reduced the cooling rate, along with the reduction in conduction transfer rate to the base plate, once temperature gradient is concentrated and behave in wall plane, with a predominant bidimensional heat transfer passing along all deposited wall firstly to dissipates on substrate volume.

The heat transfer behavior was studied by Bai et al. (2018), which analyzed the heat transfer and temperature gradient for the deposition of a 21st layer in a Ti–6Al–4V titanium wall deposited using plasma process. Despite of the different process and material, both processes are classified as Direct Energy Deposition (DED) methods, and the difference are strictly applied to heat input magnitude, but with same heat transfer methodology. For the analysis of a three-dimensional numerical model, the authors presented the temperature profile and compared with single bead deposition, showing the bidirectional heat transfer along wall height has a larger gradient than a single bead example.

As a proposed solution for the cooling problem, the implementation of an active cooling method can be applied, as the near-immersion active cooling (NIAC) proposed by Silva et al. (2020). The system proposed by the authors consists of a cooling process by immersing the deposited layers into a water vat with variable water level to follow the deposition process. The results using the NIAC method showed an increase of the effective height of a twenty-three layer wall by approximated 10 mm compared with the deposition made with natural cooling (Silva et al., 2020). Another active cooling solution was presented by Hackenhaar et al. (2020), who used air jet impingement during material deposition to induce a higher convection rate. The authors used numerical analysis and validated with experimental data (using pulsed GMAW method) within control points along the wall using both natural and active cooling. With the results, it was noticeable that interlayer temperature was kept around 200 °C even for higher layers, with a higher discrepancy from the natural cooling especially after 14th layer. At 24th layer, the interlayer temperature of the sample with air impingent was 200 °C compared with the 240 °C from the natural cooling.

Despite of that, the deposition process was satisfactory, resulting in a regular height along all geometry. The results shows that the WAAM method can achieve a good deposition accuracy and the configuration can be used for the manufacturing of larger components. Compared to Ermakova et al. (2020), who applied CMT process with oscillated strategy for the same material composition (ER70S-6 wire with 1.2 mm diameter) and similar TTS to obtain a wider wall, both samples obtained stable height along all length, with the final parameters reached as an alternative way to deposited material, aiming for thinner structures.

4. Conclusions

This work had the objective of studying the CMT process and adjusting the deposition parameters to obtain better layer build up geometry and bead geometry. The study consisted of 4 deposition groups where each one focused on individual parameter qualitative analysis of power supply current, torch travel speed, CTWD, and deposition strategy. All samples deposited were rated by geometry, surface finish, and heat input aspects. The parameters that produced the best results were applied on the deposition of a one-hundred-layer wall. Based on the results, it is possible to conclude that:

- The bidirectional deposition equals heat input along all layer length, leading to homogeneous measurements of height and width of the fabricated part. However, the regions where the torch changes direction for continuous deposition are subjected to higher heat stress and possibility of defects formation.
- The setup selected for the one-hundred-layer wall, based on all samples analyses, uses a current configuration of 65 A, with a wire feed speed of 2.6 m/min, horizontal and vertical torch travel speed respectively as 8 mm/s and 24 mm/s.
- The natural cooling is shown to be inefficient for the uninterrupted deposition of taller parts for the layer length of 160 mm. On the 100-layers wall, the natural cooling limited wall quality, lowering layer height above approximately the fiftieth layer, thus resulting in a growing CTWD, since the programmed step-over distance was constant.

Funding

No funding was received for this work.

Authors contributions

Novelino: Methodology, Investigation, Writing – original draft.
Carvalho: Methodology, Writing – review & editing.
Ziberov: Conceptualization, Writing – review & editing, Supervision.

Crosscheck

No previous publications on this dataset exist.

Declaration of competing interest

The authors declare that they have no known competing financial interests or personal relationships that could have appeared to influence the work reported in this paper.

Data availability

No data was used for the research described in the article.

Acknowledgments

The authors thank the University of Brasilia for the laboratorial infrastructure and technical support.

References

Aldalur, E., Veiga, F., Suárez, A., Bilbao, J., Lamikiz, A., 2020. High deposition wire arc additive manufacturing of mild steel: strategies and heat input effect on microstructure and mechanical properties. J. Manuf. Process. 58 (September), 615–626. https://doi.org/10.1016/j.jmapro.2020.08.060.

Anand, M., Bishwakarma, H., Kumar, N., Ujjwal, K., Kumar Das, A., 2022. Fabrication of multilayer thin wall by WAAM technique and investigation of its microstructure and mechanical properties. Mater. Today Proc. 56, 927–930. https://doi.org/10.1016/J.MATPR.2022.02.542.

Artaza, T., Suárez, A., Veiga, F., Braceras, I., Tabernero, I., Larrañaga, O., Lamikiz, A., 2020. Wire arc additive manufacturing Ti6Al4V aeronautical parts using plasma arc welding: analysis of heat-treatment processes in different atmospheres. J. Mater. Res. Technol. 9 (6), 15454–15466. https://doi.org/10.1016/j.jmrt.2020.11.012.

Bai, X., Colegrove, P., Ding, J., Zhou, X., Diao, C., Bridgeman, P., roman Hönnige, J., Zhang, H., Williams, S., 2018. Numerical analysis of heat transfer and fluid flow in multilayer deposition of PAW-based wire and arc additive manufacturing. Int. J. Heat Mass Tran. 124, 504–516. https://doi.org/10.1016/j.ijheatmasstransfer.2018.03.085.

Campatelli, G., Montevecchi, F., Venturini, G., Ingarao, G., Priarone, P.C., 2020. Integrated WAAM-subtractive versus pure subtractive manufacturing approaches: an

energy efficiency comparison. International Journal of Precision Engineering and Manufacturing - Green Technology 7 (1), 1–11. https://doi.org/10.1007/s40684-019-00071-y.

DebRoy, T., Wei, H.L., Zuback, J.S., Mukherjee, T., Elmer, J.W., Milewski, J.O., Beese, A. M., Wilson-Heid, A., De, A., Zhang, W., 2018. Additive manufacturing of metallic components – process, structure and properties. Prog. Mater. Sci. 92, 112–224. https://doi.org/10.1016/j.pmatsci.2017.10.001.

Dhinakaran, V., Ajith, J., Fathima Yasin Fahmidha, A., Jagadeesha, T., Sathish, T., Stalin, B., 2020. Wire Arc Additive Manufacturing (WAAM) process of nickel based superalloys – a review. Mater. Today Proc. 21 (xxxx), 920–925. https://doi.org/10.1016/j.matpr.2019.08.159.

Ermakova, A., Mehmanparast, A., Ganguly, S., Razavi, J., Berto, F., 2020. Investigation of mechanical and fracture properties of wire and arc additively manufactured low carbon steel components. Theor. Appl. Fract. Mech. 109 (May), 102685 https://doi.org/10.1016/j.tafmec.2020.102685.

Hackenhaar, W., Mazzaferro, J.A.E., Montevecchi, F., Campatelli, G., 2020. An experimental-numerical study of active cooling in wire arc additive manufacturing. J. Manuf. Process. 52 (January), 58–65. https://doi.org/10.1016/j.jmapro.2020.01.051.

Jafari, D., Vaneker, T.H.J., Gibson, I., 2021. Wire and arc additive manufacturing: opportunities and challenges to control the quality and accuracy of manufactured parts. Mater. Des. 202, 109471 https://doi.org/10.1016/j.matdes.2021.109471.

Laghi, V., Palermo, M., Gasparini, G., Alena Girelli, V., Trombetti, T., 2019. Geometrical characterization of wire-and-Arc Additive manufactured steel element. Adv. Mater. Lett. 10 (10), 695–699. https://doi.org/10.5185/amlett.2019.0019.

Liberini, M., Astarita, A., Campatelli, G., Scippa, A., Montevecchi, F., Venturini, G., Durante, M., Boccarusso, L., Minutolo, F.M.C., Squillace, A., 2017. Selection of optimal process parameters for wire Arc Additive manufacturing. Procedia CIRP 62, 470–474. https://doi.org/10.1016/j.procir.2016.06.124.

Martina, F., Mehnen, J., Williams, S.W., Colegrove, P., Wang, F., 2012. Investigation of the benefits of plasma deposition for the additive layer manufacture of Ti–6Al–4V. J. Mater. Process. Technol. 212 (6), 1377–1386. https://doi.org/10.1016/j.jmatprotec.2012.02.002.

Nagasai, B.P., Malarvizhi, S., Balasubramanian, V., 2022. Effect of welding processes on mechanical and metallurgical characteristics of carbon steel cylindrical components made by wire arc additive manufacturing (WAAM) technique. CIRP Journal of Manufacturing Science and Technology 36, 100–116. https://doi.org/10.1016/j.cirpj.2021.11.005.

Ngo, T.D., Kashani, A., Imbalzano, G., Nguyen, K.T.Q., Hui, D., 2018. Additive manufacturing (3D printing): a review of materials, methods, applications and challenges. Compos. B Eng. 143, 172–196. https://doi.org/10.1016/j.compositesb.2018.02.012.

Rodrigues, T.A., Duarte, V., Avila, J.A., Santos, T.G., Miranda, R.M., Oliveira, J.P., 2019. Wire and arc additive manufacturing of HSLA steel: effect of thermal cycles on microstructure and mechanical properties. Addit. Manuf. 27 (February), 440–450. https://doi.org/10.1016/j.addma.2019.03.029.

Seow, C.E., Zhang, J., Coules, H.E., Wu, G., Jones, C., Ding, J., Williams, S., 2020. Effect of crack-like defects on the fracture behaviour of wire + arc additively manufactured nickel-base alloy 718. Addit. Manuf. 36 (June), 101578 https://doi.org/10.1016/j.addma.2020.101578.

Silva, L.J., Souza, D.M., de Araújo, D.B., Reis, R.P., Scotti, A., 2020. Concept and validation of an active cooling technique to mitigate heat accumulation in WAAM. Int. J. Adv. Manuf. Technol. 107 (5–6), 2513–2523. https://doi.org/10.1007/s00170-020-05201-4.

Wang, Y., Xu, X., Zhao, Z., Deng, W., Han, J., Bai, L., Liang, X., Yao, J., 2021. Coordinated monitoring and control method of deposited layer width and reinforcement in WAAM process. J. Manuf. Process. 71 (August), 306–316. https://doi.org/10.1016/j.jmapro.2021.09.033.

Wu, B., Pan, Z., Ding, D., Cuiuri, D., Li, H., Xu, J., Norrish, J., 2018. A review of the wire arc additive manufacturing of metals: properties, defects and quality improvement. J. Manuf. Process. 35 (February), 127–139. https://doi.org/10.1016/j.jmapro.2018.08.001.

Xiong, J., Zhang, G., 2014. Adaptive control of deposited height in GMAW-based layer additive manufacturing. J. Mater. Process. Technol. 214 (4), 962–968. https://doi.org/10.1016/j.jmatprotec.2013.11.014.

Yamba, P., Zhenying, X., Yun, W., Rong, W., Xing, Y., 2019. Investigation of humping defect formation in a lap joint at a high-speed hybrid laser-GMA welding. Results Phys. 13 (February), 102341 https://doi.org/10.1016/j.rinp.2019.102341.